



Cite this: *Phys. Chem. Chem. Phys.*,
2015, 17, 8148

Cofilin reduces the mechanical properties of actin filaments: approach with coarse-grained methods

Jae In Kim,^{†a} Junpyo Kwon,^{†a} Inchul Baek,^a Harold S. Park^b and Sungsoo Na^{*a}

An actin filament is an essential cytoskeleton protein in a cell. Various proteins bind to actin for cell functions such as migration, division, and shape control. ADF/cofilin is a protein that severs actin filaments and is related to their dynamics. Actin is known to have excellent mechanical properties. Binding cofilin reduces its mechanical properties, and is related to the severing process. In this research, we applied a coarse-grained molecular dynamics simulation (CGMD) method to obtain actin filaments and cofilin-bound actin (cofilactin) filaments. Using these two obtained models, we constructed an elastic network model-based structure and conducted a normal mode analysis. Based on the low-frequency normal modes of the filament structure, we applied the continuum beam theory to calculate the mechanical properties of the actin and cofilactin filaments. The CGMD method provided structurally accurate actin and cofilactin filaments in relation to the mechanical properties, which showed good agreement with the established experimental results.

Received 30th December 2014,
Accepted 17th February 2015

DOI: 10.1039/c4cp06100d

www.rsc.org/pccp

Introduction

Actin filaments, which are abundant and major components of the cellular cytoskeleton, play essential roles in various cellular functions such as migration, division, and shape control.^{1–5} Actin filaments are polymerized with ATP-actin monomers into helix-type filaments in a polymerization process, and the ATP-actin monomers in actin filaments are changed into ADP-actin after activation.^{2,6} Because actin filament polymerization only deals with ATP-actin monomers and the catalytic action that changes ADP-actin into ATP actin requires the separation of ADP-actin monomers, the process of separating the ADP-actin monomers from the filaments is truly essential in the actin polymerization process.^{7,8}

ADF/cofilin is the protein that severs actin filaments and enhances the motility and dynamics of filament assembly.^{9–11} Cofilin can sever actin filaments and create numerous free filaments, which are available for polymerization or depolymerization, and this binding induces some conformational changes in the actin filaments.¹² This means that the structural changes in the actin filaments caused by the cofilin binding might automatically change the mechanical properties of the filaments.

Several experimental studies have predicted the mechanical properties of actin filaments.^{13,14} However, some of these estimates were restricted by experimental limitations and the lack of detailed information about the cytoskeletal ultrastructure, and the need to analyze the protein on temporal scales

ranging from picoseconds to nanoseconds has gained importance as the proteins are exposed to thermal fluctuations in real physiological surroundings.^{15,16}

As an alternative method for determining the protein's dynamics, a simulation such as molecular dynamics (MD) makes it possible to elucidate the details of molecular motions.¹⁷ The use of an MD simulation makes it possible to understand the axial and torsional stiffness of short actin fibrils.^{1,15} In addition, a steered MD (SMD) simulation of stretching actin caused the twisting of an actin filament. In particular, a small change in the twisting angle has been shown. However, opposite angle change directions were found for cofilactin and actin.¹ This showed that the binding of cofilin results in a change in the torsional behavior of actin filaments.

However, an MD simulation of an all-atom approach might be still computationally inefficient when treating a very large system despite recent advances in computer technology.^{18–20} In particular, when analyzing actin molecules, an all-atom MD simulation is hard to use for equilibrating their statuses, because their sizes are large (50 556 atoms or 722.214 kDa for cofilactin PDB: 3J0S), and a very long computational calculation time would be needed. To simultaneously equilibrate proteins from the Protein Data Bank (PDB) and maximize the efficiency of the calculation, something different is needed, namely a coarse-grained MD force field that is able to reduce the computational time while maintaining the high accuracy of the results.

Coarse-grained force field MARTINI is based on a four-to-one mapping.²¹ It represents an average of four heavy atoms as a single pseudo-atom while still considering only four main types of interaction sites: polar (P), nonpolar (N), apolar (C), and charged (Q), in order to keep the model simple.²² Because MARTINI is able

^a Department of Mechanical Engineering, Korea University, Seoul 136-701, Republic of Korea. E-mail: nass@korea.ac.kr

^b Department of Mechanical Engineering, Boston University, Boston, MA 02215, USA

[†] These authors (J.I.K. and J.K.) made equal contributions to this work.

to reduce the number of atoms and simplify the force field of both proteins and water molecules, which make up a critical portion of the total number of atoms, the calculation time for very large proteins (cofilactin and actin filaments) is dramatically shortened, and two separate simulations can be conducted in a very harmonious way.

The idea of an elastic network model (ENM) was proposed in the 1990s as another method for examining proteins by representing the dynamics and conformations of proteins and molecules.^{23–26} As mentioned above, MD simulations have restrictions when used to calculate the interactions of all the atoms contained in proteins and molecules, and a compromise between the accuracy and time efficiency exists. However, it can achieve plausible analysis results in a short calculation time when only alpha-carbon atoms, which are important in forming a protein as a backbone, are extracted from the PDB data for analyzing the globular motion of proteins.²⁷ Currently, the interactions of the pairs of alpha-carbon atoms located within a distance shorter than the cutoff distance are regarded as linear springs with a generic force constant. Despite the simplicity of ENM, they have been applied in various studies of protein dynamics for a decade. Computational studies with ENM have been used to calculate the low-frequency normal modes of proteins in order to describe the conformational changes related to protein functions,^{28–38} as well as to measure the mechanical properties of various cytoskeletal proteins or neurodegenerative amyloid fibrils within acceptable ranges.^{39–41} It should be mentioned that, although of an evident importance, to the best of author's knowledge, no such computational studies regarding the difference of mechanical properties between a pure actin filament and cofilactin filament have been found in previous references.

In this study, we analyzed how actin filaments experience conformational changes induced by the binding of cofilins and determined whether this conformational change could affect the mechanical properties, including the torsional modulus of actin filaments. In order to compare the structural differences, two separate simulations were conducted, one for cofilactin filaments and another for actin filaments. A coarse-grained MD simulation was used to avoid the long computational time needed because of the huge size of the actin filament. After the simulation, the actin and cofilactin filaments were remodeled by lengths based on the coarse-grained MD simulation results, and their mechanical properties were analyzed using ENM and normal mode analysis (NMA). Finally, we calculated the mechanical properties of the actin filaments and compared these to experimental results. We found that the ADF/cofilin made the actin filaments flexible for bending and torsion. In addition, the Young's modulus and torsional modulus of the cofilactin filaments were much lower than those of actin filaments.

Materials and methods

Materials

Among the numerous possible types and statuses based on factors that include the organism, binding states, and sizes, cofilactins, which are a complex of cofilins bound to actin

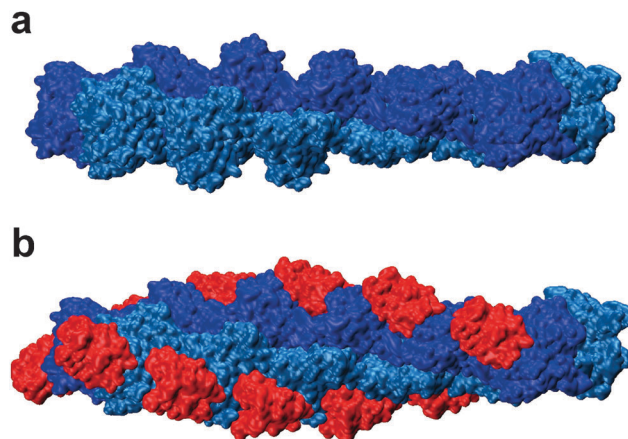


Fig. 1 Actin and cofilactin structural models used in the coarse-grained MD simulations. (a) Actin filament, (b) cofilactin filament. Both filaments are obtained from PDB with PDB code of 3J0S.

filaments, are used to compare the mechanical properties of pure actin filaments and cofilactin filaments. That is, two cases, one for cofilactin and another for actin, have to be simulated independently in order to compare the conformational changes that lead to different mechanical properties. When preparing two discrete simulations, it would be ideal to find the protein information for cofilactin and actin filaments under exactly the same conditions.

However, it is difficult to find the protein information for cofilactin and actin filaments with the status and type. Therefore, the protein data for cofilactin filaments containing 12 actin subunits and 12 cofilin subunits with a length of ~ 27 nm found in the PDB were selected for use in a cofilactin simulation (shown in Fig. 1b), and the same protein that only contained 12 actin subunits without the 12 cofilin subunits was used for the actin simulation (presented in Fig. 1a). A 9.0 Å resolution cryo-electron microscopic three-dimensional reconstruction of the cofilin-decorated actin filaments was obtained from the PDB with a PDB code of 3J0S. The initial structures of the cofilactin were taken from Galkin *et al.*⁴² and contained both actin cytoplasmic derived from *Gallus gallus* and cofilin-2 from *Homo sapiens*. The resolution of the PDB is quite low, but its atomic positions are based on high resolution structures⁴² and our CGMD approach is less dependent on the detailed atomic positions. All of the structural representations are done with VMD.⁴³

Methods

Coarse-grained molecular dynamics simulation (CGMD). Using information from the PDB without any treatment could cause problems because the protein structures extracted from the PDB could be distorted by the experimental conditions and techniques, although the protein data could be used directly for constructing suitable structures for an ENM analysis.⁴⁴ Furthermore, the atomic structures of pure actin filaments have to be different from those of cofilactin filaments depending on whether or not the cofilins are bound into the actin filaments.

Because we started with considering the PDB data for cofilactin, the cofilin removed pure actin structure was not an energetically and structurally appropriate pure actin structure. To obtain more reliable position data for the actin filaments, two separate MD simulations had to be conducted for the pure actin and cofilactin. Therefore, the protein structures from the PDB had to be relaxed and equilibrated by applying the MD simulation to enhance the reliability of the research results.

An MD simulation makes it possible to obtain reliable atomic structures using the PDB data for both pure actin and cofilactin. However, the actin filaments have a large size and a large degree of freedom (50 556 atoms or 722.214 kDa for cofilactin 3J0S), which causes difficulties in relation to the need for a long computational time and large amount of computational resources. To overcome this problem, we applied CGMD using MARTINI.^{21,22} Applying MARTINI allowed us to reduce the degree of freedom of the actin filaments to about one fourth compared to the all-atom structure, as shown in Fig. 2a and b. Depending on the amino-acid's size and type, MARTINI describes one amino-acid with around one to five pseudo atoms. MARTINI version 2.4 and force field MARTINI 21p were used for two simulations *via* GROMACS version 4.6.5,^{45–48} one for cofilactin and the other for actin. First, coarse-grained pdb files and topology files were created using the original pdb data and dssp files. Then, a water box was set using polarized water molecules having 1 nm dimension from the end of the cofilactin and actin filaments. We chose the polarized water file because the electrostatic interactions between atoms had to be considered to obtain a reasonable output from the simulation.⁴⁹ Finally, CGMD simulations were conducted under periodic boundary conditions (PBC) at a constant temperature ($T = 298$ K). A free dynamics simulation of the entire system was performed for 40 ns with 2 fs time step and 20 000 000 steps to obtain the equilibrium structure.

Elastic network model (ENM). We applied an ENM to analyze the fluctuation behavior of the actin and cofilactin obtained in the CGMD simulations. Seven models of different length were built with the final position data from CGMD using ENM. The ENM considered alpha-carbon atoms to represent the residue of a protein, and the actin constructed using only alpha-carbons is shown in Fig. 2c. The interaction of the alpha-carbon atoms can be described using the harmonic potential energy. This interaction is defined by connecting a pair of atoms using linear springs with lengths shorter than the cut-off distance, as depicted in Fig. 2d.

After connecting all the suitable alpha-carbon atoms, we can evaluate the overall conformational potential of the structure. The potential energy V for an ENM connected using harmonic springs with a force constant γ is given by

$$V = \frac{\gamma}{2} \sum_{i=1}^N \sum_{j \neq i}^N (r_{ij} - r_{ij}^0)^2 \quad (1)$$

where N represents the total number of residues, r_{ij} is the distance between two residues i and j , and superscript 0 stands for the equilibrium conformational state.

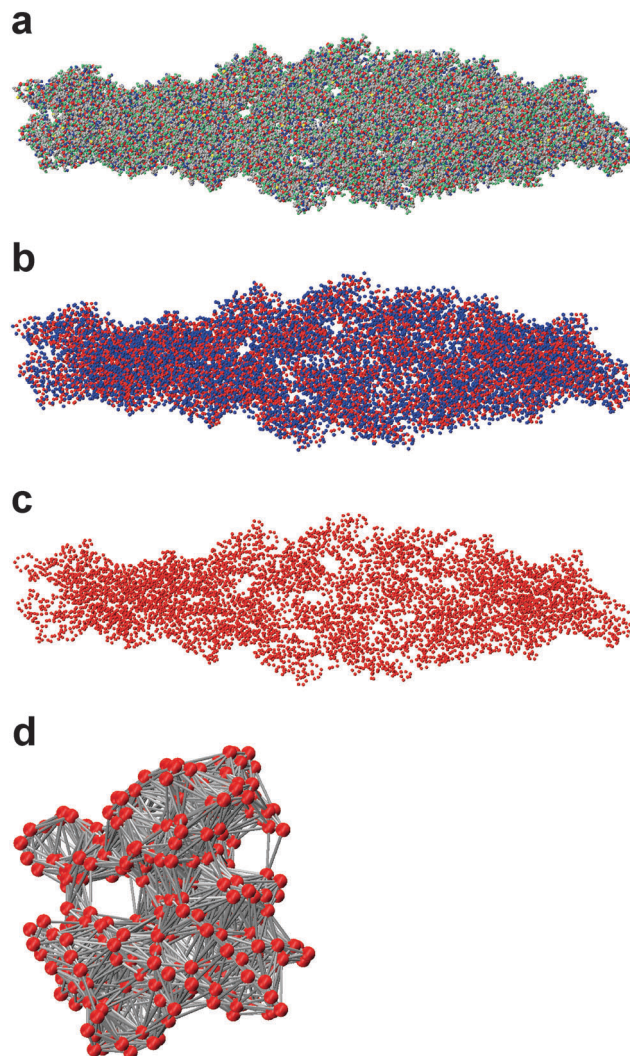


Fig. 2 Visualization of creating an elastic network model. (a) The original cofilactin structure composed of all atoms, (b) coarse-grained model by using force field martini21p (four-to-one mapping), (c) coarse-grained model reduced to just the alpha-carbon atoms, (d) zoom-in view of the elastic network model (c) composed of alpha-carbon atoms which linear springs are connected between.

In order to analyze the fluctuation dynamics of protein structures *via* an ENM, the Gaussian network model (GNM) was first introduced. In this model, residues were assumed to experience Gaussian-distributed fluctuations about their mean positions; results using this model have successfully connected with experimental data.^{24,50} However, a GNM has limitations when used to predict three-dimensional fluctuations, because it is based on a one-dimensional model for evaluating the mean-square displacements and cross-correlations between fluctuations.²⁷ Therefore, an extended model containing three-dimensional information about the residues, an anisotropic network model (ANM), is generally applied. (We use the ENM to replace the ANM after this because we are only considering a three-dimensional model.) The stiffness matrix of the ENM can be calculated through second derivations of the potential energy in terms of x , y , and z . The second derivatives of the potential

energy of each pair, h_{ij} , becomes a 3×3 matrix having nine components. Finally, the Hessian matrix \mathbf{H} can be written as:

$$h_{ij} = \begin{bmatrix} \frac{\partial^2 V}{\partial X_i \partial X_j} & \frac{\partial^2 V}{\partial X_i \partial Y_j} & \frac{\partial^2 V}{\partial X_i \partial Z_j} \\ \frac{\partial^2 V}{\partial Y_i \partial X_j} & \frac{\partial^2 V}{\partial Y_i \partial Y_j} & \frac{\partial^2 V}{\partial Y_i \partial Z_j} \\ \frac{\partial^2 V}{\partial Z_i \partial X_j} & \frac{\partial^2 V}{\partial Z_i \partial Y_j} & \frac{\partial^2 V}{\partial Z_i \partial Z_j} \end{bmatrix} \quad (2)$$

$$\mathbf{H} = \begin{bmatrix} h_{11} & h_{12} & \cdots & h_{1N} \\ h_{21} & & & h_{2N} \\ \vdots & & & \vdots \\ h_{N1} & & & h_{NN} \end{bmatrix} \quad (3)$$

Because the Hessian matrix is the system's stiffness matrix, the vibrational characteristics of the system can be easily analyzed using a NMA such as $\mathbf{H}\mathbf{q} = \mathbf{m}\omega^2\mathbf{q}$ where \mathbf{m} is the mass matrix of the protein structure, and ω and \mathbf{q} represent the natural frequency and its corresponding eigen-mode, respectively. As mentioned in obtaining the Hessian matrix, each pair has a 3×3 matrix. The Hessian matrix has a size of $3N \times 3N$, which is the same as \mathbf{m} and \mathbf{q} . The result has six zero modes, which represent six rigid body motions of the system, such as the translation and rotation of the system in the x , y , and z directions. The other modes correspond to specific motion characteristics of the protein depending on its globular shape, *i.e.*, bending, twisting, axial, and combinations of these. Low-frequency modes appear to have global motions, and modes with higher frequencies show local motions of the proteins. A NMA using the ENM is especially effective for depicting the global motion of the protein without considering the detailed chemical interactions. In particular, for filamentous structures, *i.e.*, f-actin, amyloid fibrils, and tubulin, low-frequency modes describe specific modes, which make it possible to obtain the mechanical properties of those materials. Therefore, normally only the least number of modes, from thirty to hundreds of modes, is used to analyze a material's characteristics.

Euler beam theory. Because actin filaments and cofilactin filaments are very long relative to their circular areas, they can be modeled as cross-sectional beams. In addition, the fact that the filaments' area-to-length ratio is less than 0.1 makes it possible to apply the Euler beam theory. In the case of the free vibration of a system, the equation of motion for the bending and torsional vibration of a beam is written as follows:^{51–53}

$$\frac{\partial^2 w(x, t)}{\partial t^2} + \frac{E_B I}{\rho A} \frac{\partial^4 w(x, t)}{\partial x^4} = 0, \quad \text{for the bending mode} \quad (4a)$$

$$\frac{\partial^2 \theta(x, t)}{\partial t^2} + \frac{G_t}{\rho} \frac{\partial^2 \theta(x, t)}{\partial x^2} = 0, \quad \text{for the torsional mode} \quad (4b)$$

where w and θ are the transverse displacement for the bending mode and the torsional angle for the torsional mode, respectively; and x is defined along the longitudinal direction of a filament. In addition, ρ is the mass density, A is the cross-sectional area of a filament, E_B is the bending elastic modulus, I is the second moment of inertia, and G_t is the torsional shear modulus.

In order to solve the equation mathematically, the variables should be separated as follows: $w(x, t) = z(x)t(t)$, $\theta(x, t) = \phi(x)t(t)$. Then, the original equations for each motion are changed into the following:

$$\frac{E_B I}{\rho A} \frac{d^4 z}{dx^4} - \omega_b^2 z = 0, \quad \text{for the bending mode} \quad (5a)$$

$$\frac{G_t}{\rho} \frac{d^2 \phi}{dx^2} - \omega_t^2 \phi = 0, \quad \text{for the torsional mode} \quad (5b)$$

where $\omega_b^2 = \frac{\beta_n^4 E_B I}{\rho A}$; $\omega_t^2 = \left(\frac{n\pi}{L}\right)^2 \frac{G_t}{\rho}$; ω_b and ω_t are the natural frequencies for the bending and torsional modes, respectively; and n and β_n are the mode index and mode index-dependent constant, respectively. Therefore, the mode shapes for each deformation mode are defined as follows:

$$z(x) = A_n^B [\cosh \beta_n x + \cos \beta_n x - \sigma_n (\sinh \beta_n x + \sin \beta_n x)], \quad \text{for the bending mode} \quad (6a)$$

$$\phi(x) = A_n^T \cos \frac{n\pi x}{L}, \quad \text{for the torsional mode} \quad (6b)$$

where the constants $\sigma_n = 0.98$, and $\beta_n L = 4.37$. Finally, the mechanical properties are related to the natural frequencies for each mode as follow:

$$E = \frac{\rho A}{\beta_n^4 I} (\omega_1^b)^2, \quad \text{for bending} \quad (7a)$$

$$G_t = \frac{\rho}{\pi^2} (\omega_1^t)^2 L^2, \quad \text{for torsion} \quad (7b)$$

Using calculated G_t and polar moment of inertia J we can calculate torsional rigidity (C) as $C = G_t J$. These equations demonstrate that the mechanical properties such as Young's modulus and the torsional modulus of the system can be easily computed using the above Euler-beam theory once the frequencies are obtained from the NMA.

Results

Equilibration and structural change

We performed a 40 ns equilibration simulation with CGMD using the previously mentioned pure actin filament and cofilactin filament. Fig. 3 shows the root mean square deviation (RMSD) and energy results from this equilibration simulation of our two models. The RMSDs of the pure actin filament and cofilactin filament indicate a structural difference between these two models. As shown in Fig. 3a, the pure actin filament had an RMSD of about 1.2 nm, while cofilactin had a value of ~ 1.0 nm (Fig. 3b). Both models were prepared using the same PDB data, which contained cofilin bound to actin filaments. It is obvious that the pure-actin filament showed a larger RMSD than the cofilactin due to the elimination of the cofilin bound to the actin, as we expected. In addition, the total energy values of both models were calculated to examine whether or not these two models were energetically stable. The results are depicted in Fig. 3c and d, which exhibit stable energy behaviors for both structures.

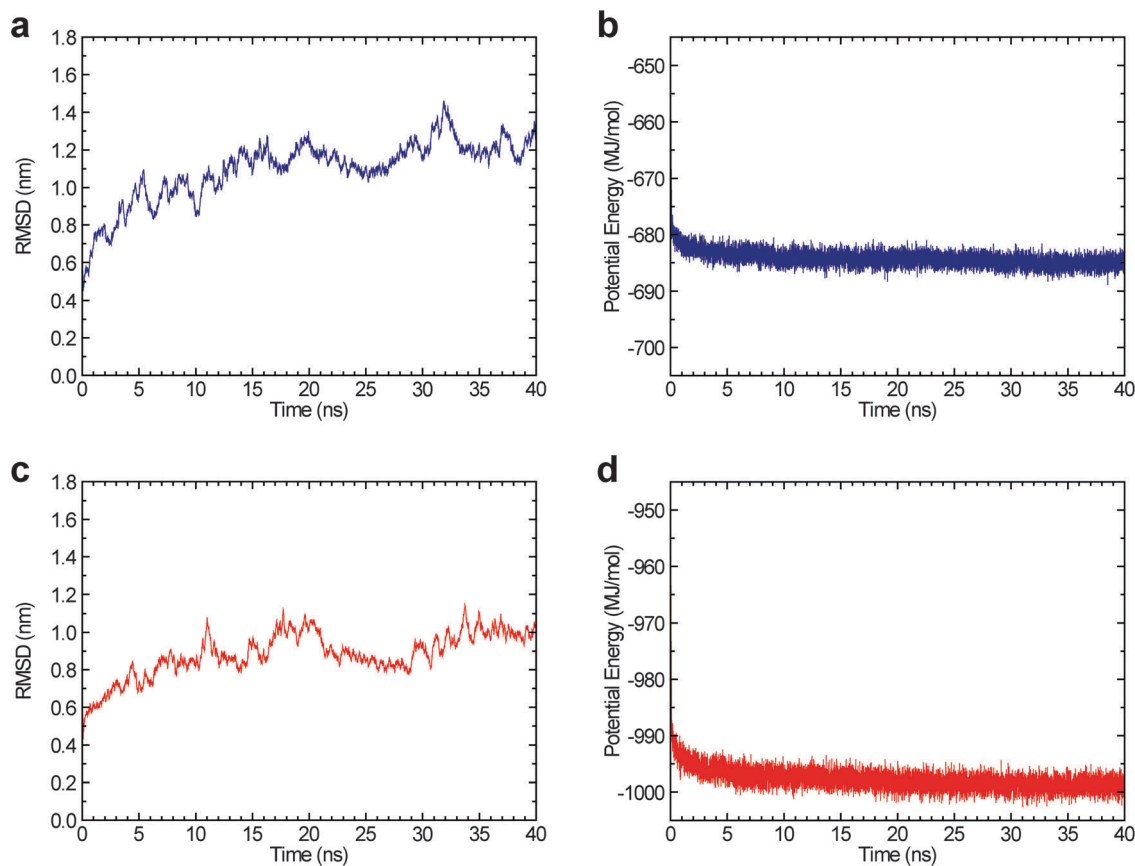


Fig. 3 Equilibrium simulation results for actin and cofilactin structures. (a) and (b) show plots of RMSD fluctuation and potential energy of the actin filament. (c) and (d) show the same plots of the cofilactin filament. Two simulations are guaranteed with having saturated RMSD and potential energy during computations for 40 ns.

Clearly, the total energy values of the pure actin filament and cofilactin filament were different, which depended on the conformation of each actin monomer and whether or not the cofilin was bound.

In the 40 ns equilibrium simulation, the conformational differences between the pure actin filament and cofilactin filament were observed after ensuring the energy minimization and protein dynamics. Fig. 4a and b show the pure actin filament and cofilactin filament after the equilibrium simulation, respectively. The structural change is identified in comparison with Fig. 1. A comparison of the pure actin filaments in Fig. 1a and 4a depicts that the shape of the external area has changed, which indicates that each monomer experienced a conformational change after the cofilin was eliminated. The cofilactin shows a bent conformation after the equilibrium simulation, which seems to be the effect of cofilin binding. The structural changes in these two models were confirmed, but we had to measure the difference between the two models to build longer fibril models. The structural changes in the centroids of each chain were continually determined. Then, we could categorize the conformational characteristics between these filaments using three variables: the distance between monomers (δ), twisting angle (θ), and tangential angle (φ), which are depicted in Fig. 4d with details. Here, the twisting

angle indicates how each layer is twisted, and the tangential angle represents how much the entire filament is rotated with respect to the major axis, respectively.

These three values of parameters were measured for the two models, and the results are listed in Table 1. When monitoring the conformational change, the three values for the actin filament were all less than those for the cofilactin filament. The coarse-grained MD simulation results indicated that the actin filament was much straighter than the cofilactin, as the cofilin causes twisting of the bare actin filament and makes some clefts through interaction with the actin monomers. The greater twisting of the cofilactin indicated that it could have more torsional flexibility than the pure actin filament, which will be confirmed later, while the change in the tangential angle also implied a smaller Young's modulus for the cofilactin filament. These conformational changes due to the binding of cofilin seemed to lead to changes in mechanical properties such as the bending modulus and torsional modulus of the actin filament. The straightness of the filaments can also be measured by calculating the correlation factor (C_s), which is defined as follows:

$$\langle C_s \rangle = \left\langle \cos \left[\varphi(s) - \varphi(0) \right] \right\rangle = e^{-\frac{s}{2L_p}} \quad (8)$$

where s is the segment contour length of a filament, φ is the tangential angle, L_p is the persistence length, and its value

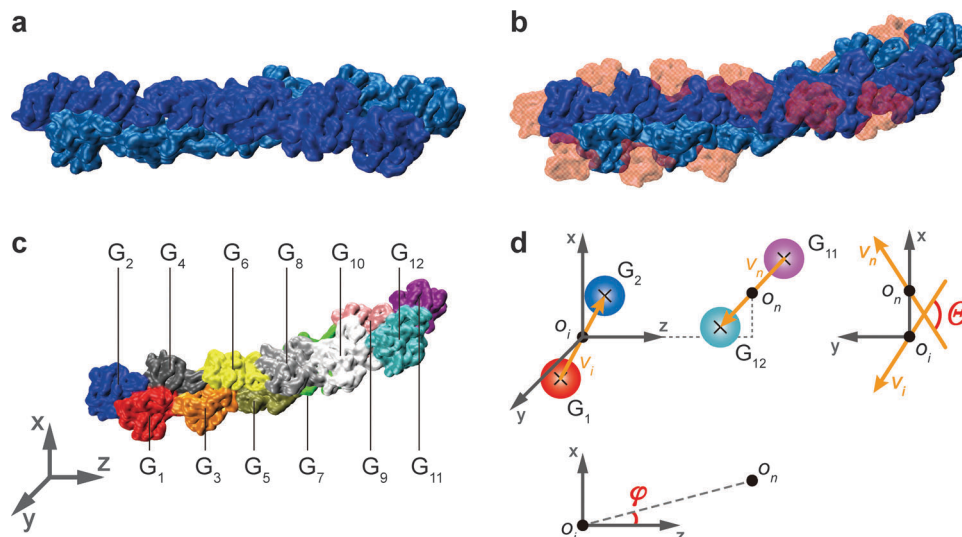


Fig. 4 Conformation change results after coarse-grained MD simulation. (a) Visualization of the actin filament after equilibrium, (b) visualization of the cofilactin filament. Even though (a) and (b) have identical calculation conditions, conspicuous structural differences have been noticed. (c) and (d) contain basic information and explain definitions to illustrate conformational changes. (c) Shows 12 actin monomers (G_n) in one filament, (d) represents the tangential angle (φ) from the z -axis and twisting angle (θ) calculated from vectors (V_i , V_n) of each monomer.

Table 1 Main parameters of characteristics showing actin and cofilactin structural transitions after the simulations

Parameters	Actin	Cofilactin
Distance, δ (\AA)	50.06	52.25
Tangential angle, φ (deg)	0	10.68
Correlation factor, C_s	1.000	0.983
Twisting angle, θ (deg)	30.68	42.15

defines the L_p -dependence of the tangential angle. The CGMD results showed that the correlation factor of the actin filament was saturated to one, whereas it decreases to 0.983 for cofilactin. This corresponded to the previous experimental and computational results proposing that filament subunits with bound cofilins are less flat and maintain significantly more open nucleotide spaces than bare filament subunits, which could be one of the main changes caused by cofilin and make the actin filaments more flexible in bending and torsion.^{54–56}

As proteins were equilibrated with saturated RMSD fluctuations, and major dynamic changes were simultaneously observed, we could stack their monomers into filaments with different lengths. We produced seven filament samples with lengths of 25–180 nm for each case when preparing the ENM and NMA. Here, we produced cofilactin filaments by stacking only actin monomers after the interaction of cofilins *via* CGMD simulation, because we wanted to verify the effect of the cofilin on the actin filaments in relation to the conformational change and mechanical properties induced by the shape difference. In order to consider all the interactions between the surrounding atoms and environment, monomers G_7 and G_8 (depicted in Fig. 4c) positioned in the middle were used as the basic elements, and all the results from the CGMD simulation were considered.

Vibrational modes of cofilactin and actin

Eigenvalues and eigenvectors can be obtained by solving eigenvalue problems using Hessian matrices. Then eigenvectors were analyzed individually to determine the bending and torsion modes. As shown in Fig. 5, in a 10-layer-actin filament case ($L = 50$ nm), the major bending mode index is equal to seven, the torsional mode index is equal to ten (described in Fig. 5a), and their frequencies are around 30.7 and 90.1 GHz (depicted in Fig. 5b), respectively. These bending and torsional mode shapes are presented in Fig. 5c and d, respectively.

We analyzed the major modes by building seven different length models for the actin and cofilactin filaments. In Fig. 6, we only describe the mode index and eigenvalue for the length data of the actin filament, because the cofilactin showed similar behavior. As the length increased, the bending mode index maintained its value for the seven models, while the torsional mode index increased (Fig. 6a). This indicated that the dominant vibrational behavior of the 10-layer-actin filament was bending. The torsional mode index increased as the length increased because the various bending modes appeared as the filament became longer. It is obvious that as filament gets longer, various bending mode appears as the degree of freedom increases, which leads to increase in the number of bending modes. However, the eigenvalues in each mode were saturated at around zero as the length increased, which is described in Fig. 6b. As the actin filament exceeded 100 nm, the eigenvalues of the bending mode and the torsion mode exhibit to be stabilized. Bending mode maintained its index while the eigenvalue were stabilized, however, the torsional mode index was increased while the eigenvalue was stabilized. The eigenvalue saturations for these two major modes indicate that we may expect stable mechanical properties for actin filaments longer than ~ 100 nm.

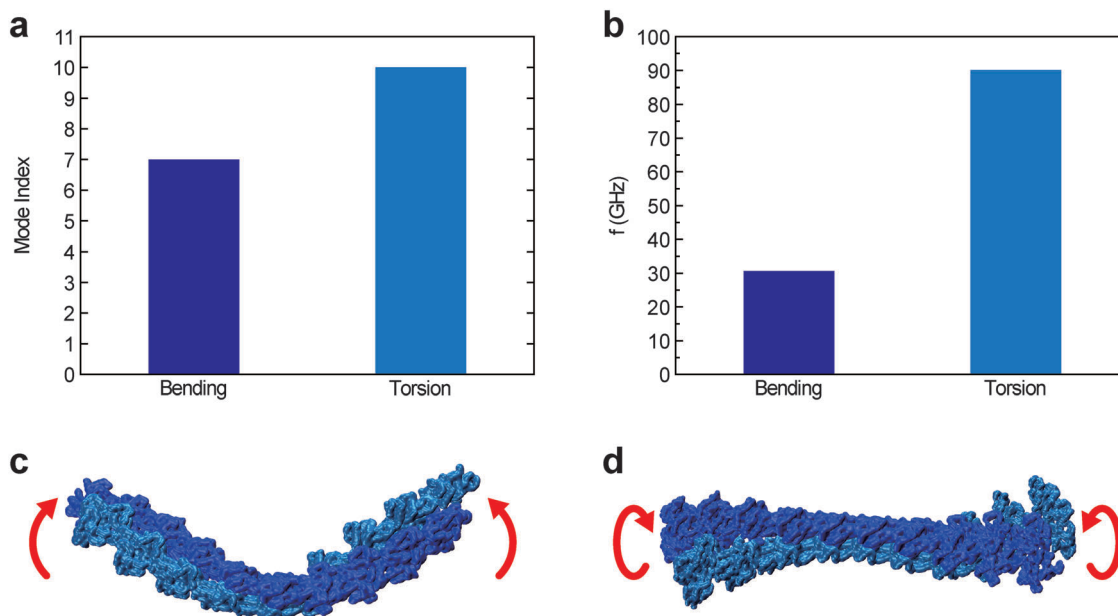


Fig. 5 The results of vibrational analysis for an elastic network model of a 10-layer-actin filament. (a) Mode indices, (b) frequencies for bending and torsion, respectively. (c) and (d) represent each mode shape.

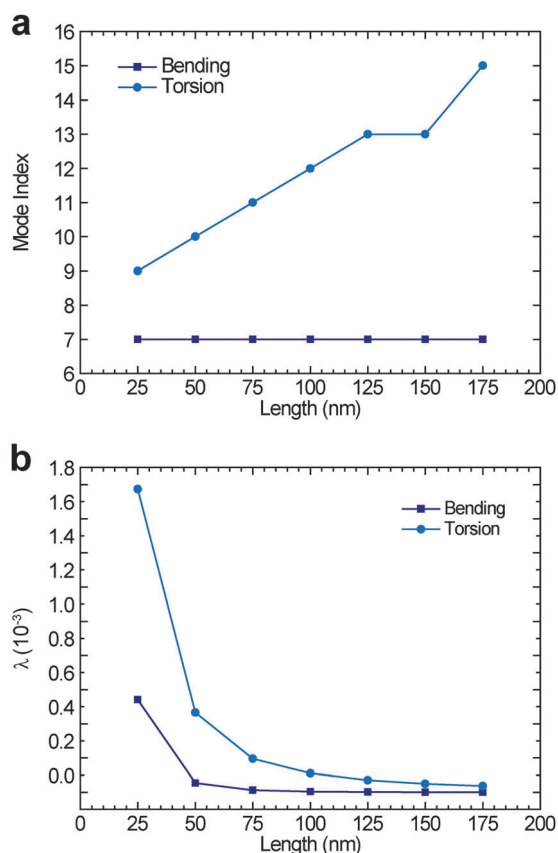


Fig. 6 Plots of mode indices and eigenvalues (λ) along the length of the actin filament. (a) Shows that the mode index of bending is equal in whole lengths and that of torsion increases as length increases. (b) Shows that eigenvalue of each mode saturates with increased lengths.

Mechanical properties of actin

Based on the ENM analysis results, the mechanical properties of each actin filament length can be calculated by applying the Euler beam theory. The axial area and the area moment of inertia of the actin filament (I) were found to be $3.92 \times 10^{-17} \text{ m}^2$ and $1.43 \times 10^{-34} \text{ m}^4$, respectively, when calculating with the previous simulation data containing position information of the filament. Thus, the persistence length (L_p), bending rigidity (EI), and torsional rigidity (C) are easily found using eqn (7) and (8). In the case of the longest actin filament in our research ($L = 180 \text{ nm}$), we have an L_p of $10.53 \text{ }\mu\text{m}$, EI of $4.50 \times 10^{-26} \text{ Nm}^2$, and C of $4.37 \times 10^{-26} \text{ Nm}^2$. These can be compared with experimental data to determine the reliability of the ENM results. Our measured data and the experimental data of other groups are listed in Table 2. Our calculated values for C and EI fit well in the known range of values for actin filaments.⁵⁷

Various groups have investigated the bending rigidity of actin filaments. Oosawa found bending rigidities of $2\text{--}7 \times 10^{-26} \text{ Nm}^2$ through either observing the thermal fluctuations of individual single filaments using a microscope or employing active micromanipulations.⁵⁸ Yanagida *et al.*, Gittes, and Ott *et al.* applied fluorescence microscopy to record the thermal fluctuation and find the bending rigidities. Yanagida *et al.* found a value of $6.5 \times 10^{-26} \text{ Nm}^2$ in the presence of Ca^{2+} and ATP by measuring the end-to-end distances and contour

Table 2 Comparison of mechanical properties of the actin filament between the results of the elastic network model and experiments

Method	ENM	Experiment
L_p (μm)	10.53	$9.8^{56} (\pm 0.14)$
EI (10^{-26} Nm^2)	4.50	$1.5\text{--}8.7^{58\text{--}65}$
C (10^{-26} Nm^2)	4.37	$0.14\text{--}8.5^{62,66\text{--}68} (\pm 1.3)$

lengths, and Gittes *et al.* and Ott *et al.* found values of $7.3(\pm 0.44) \times 10^{-26} \text{ Nm}^2$ and $6.8(\pm 0.14) \times 10^{-26} \text{ Nm}^2$ using a sophisticated Fourier-mode analysis in the presence of Mg^{2+} and an analysis of the correlation between the tangents along a filament, respectively.^{59–61} Yasuda *et al.* repeated fluorescence experiments using phalloidin-stabilized actin filaments with a tangent correlation analysis and found bending rigidities of $5.8(\pm 0.1) \times 10^{-26} \text{ Nm}^2$ with Ca^{2+} and $6.2(\pm 0.1) \times 10^{-26} \text{ Nm}^2$ with Mg^{2+} .⁶² Isambert *et al.* more thoroughly explored the influence of a nucleotide bound divalent cation, and the presence or absence of phalloidin, as well as the tropomyosin–troponin regulatory complex, and found a bending rigidity of $3.2\text{--}8.7 \times 10^{-26} \text{ Nm}^2$.⁶³ When optical tweezers were applied by Dupuis *et al.* and Riveline *et al.*, these groups found values of $1.5 \times 10^{-26} \text{ Nm}^2$ and $3.0 \times 10^{-26} \text{ Nm}^2$, respectively.^{64,65}

There are many references to the torsional rigidity of an actin filament. Tsuda *et al.* found a torsional rigidity of $8.0(\pm 1.2) \times 10^{-26} \text{ Nm}^2$ with a buffer containing Mg^{2+} rather than Ca^{2+} .⁶⁶ Yasuda *et al.* bound an actin filament in a straight configuration to two beads and then used optical tweezers. They found bending rigidities of $8.5(\pm 1.3) \times 10^{-26} \text{ Nm}^2$ with Ca^{2+} and $2.8(\pm 0.3) \times 10^{-26} \text{ Nm}^2$ with Mg^{2+} .⁶² Yoshimmura *et al.* calculated a torsional rigidity of $0.2 \times 10^{-26} \text{ Nm}^2$ by resolving the rotational motion through monitoring of the transient absorption anisotropy.⁶⁷ Finally, Prochniewicz *et al.* reported torsional rigidities of $0.14 \times 10^{-26} \text{ Nm}^2$ with Ca^{2+} and phalloidin and $0.25 \times 10^{-26} \text{ Nm}^2$ without phalloidin.⁶⁸

Various experiments have found different values for the mechanical properties of actin. However, these depend on the type of actin, experimental methods, and experimental conditions. It is necessary to focus on the range of the mechanical properties. The data gathered from experiments are listed in Table 2. Here, L_p appears to have a value of $10.53 \mu\text{m}$; EI shows values of $1.5\text{--}8.7 \times 10^{-26} \text{ Nm}^2$, which have the same order of magnitude; and C is calculated to have a range of $0.14\text{--}8.5 \times 10^{-26} \text{ Nm}^2$, which shows a difference of one order of magnitude between the minimum and maximum values. However, these ranges for the mechanical properties of actin are accepted values because of the different conditions.⁵⁷ The mechanical properties that we calculated using the ENM results are not identical to all of the experimental data. However, three properties fit the ranges of the experimental data. As previously mentioned, the important point is the range of values because the experimental data do not have exactly the same values. Our mechanical property data were calculated using the ENM, which lacked detailed chemical interactions between the side-chains of the protein. However, it has been proven that the ENM can measure the mechanical properties of fibril structures, which may be considered a beam model using the continuum theory.^{39–41} The ENM is capable of measuring the mechanical properties because it is a structure-dependent model. The simple harmonic interactions between alpha-carbons cannot describe interactions such as the van der Waals interactions and electrostatic interactions. However, it has been shown that the global motion of a structure is well depicted by applying the ENM.^{23,28–31,35,36,38,50,69} For a known case, the

low-frequency normal modes describe the global motions of proteins. In addition, the global motions for fibril-shaped structures include the bending, torsion, and axial modes. Thus, we can accurately describe these important major modes with their mechanical properties, which makes it possible to find mechanical properties of actin filaments that are similar to the experimental results.

Comparison of mechanical properties of actin and cofilactin

Many previous experiments have found that cofilin makes actin filaments flexible in bending and torsion.^{55,56,70,71} Computational approaches have also been used to study the conformational changes in actin filaments induced by cofilin, but its mechanical properties have not yet been verified *via* computational calculations. Our objective in this work was to analyze cofilin's effect on the mechanical properties of actin filaments. We compared the mechanical properties of cofilactin and actin filaments to follow up on the previous experimental work. As previously mentioned, we constructed two different models to describe the cofilactin and actin filaments using the ENM. The binding of cofilin causes a conformational change in pure actin. Thus, to measure the mechanical properties, the cofilin had to be removed. We removed the cofilin because the ENM cannot describe the chemical effect of weakening of the actin filament. All the residues were described using the alpha-carbon, and the interactions were described using only the harmonic potential, which means that the structure was actually described as a single material beam. Therefore, including cofilin in cofilactin merely involves adding a large axial area, large mass, and large stiffness compared to pure actin. Thus, we considered only the actin part from the equilibrated cofilactin structure to construct the ENM, which had a similar axial area and the same mass as the pure-actin-based ENM.

Following eqn (7) and (8), we calculated E , G , and L_p for both the cofilactin and actin filaments. The results for these three mechanical properties of the cofilactin and actin filaments are depicted in Fig. 7a–c respectively. We first calculated Young's modulus for two models with different lengths. For the actin filament, Young's modulus seemed to stabilize at around $\sim 300 \text{ MPa}$ for a length greater than 75 nm . It increased from 150 to 300 MPa when the length was increased from 25 to 75 nm . Young's modulus for the cofilactin experienced a smaller change than the actin filament. The total increase in the Young's modulus for cofilactin was approximately 40 MPa when the length was increased from 25 to 200 nm . The saturated Young's modulus values for the actin and cofilactin filaments were 300 and 175 MPa , respectively. The actin filament had a Young's modulus that was about twice that of the cofilactin filament. It was obvious that cofilin binding weakened the Young's modulus of the actin filament, as previously reported.⁵⁶ However, the Young's modulus values of our two models fit the existing range for actin.⁵⁷

We examined the torsional modulus for the actin and cofilactin filaments to investigate the effect of cofilin binding. For filamentous structures such as actin, amyloids, and tubulin, bending is a major property of interest. However, actin is a

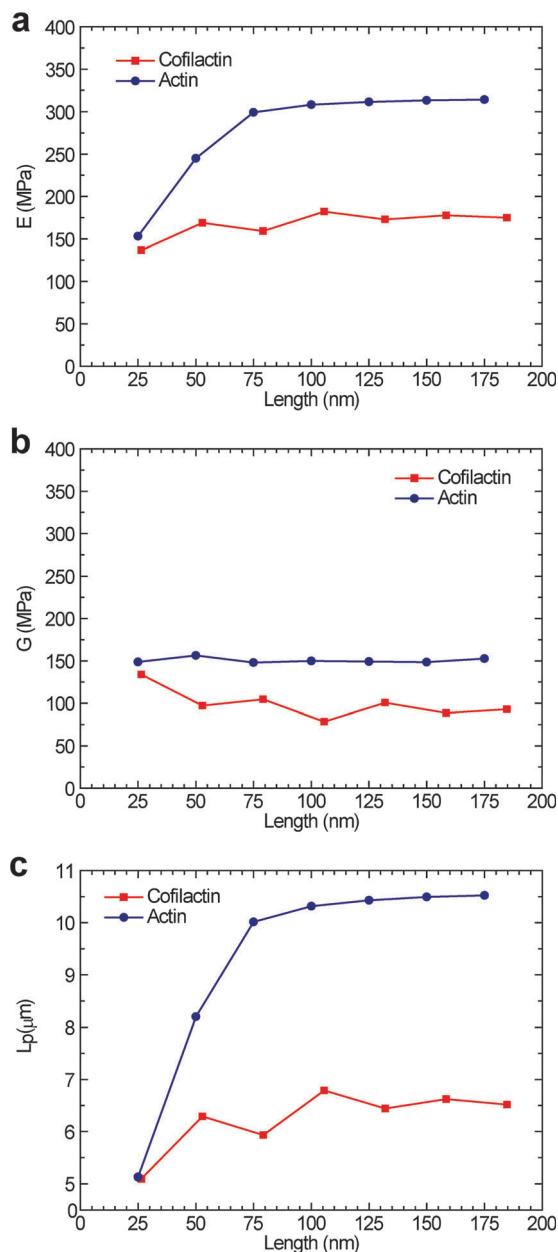


Fig. 7 Comparisons of mechanical properties between actin and cofilactin filaments. (a) Young's modulus, (b) torsional modulus, (c) persistence length with increased lengths. (a)–(c) Indicate that mechanical properties of cofilactin are less than those of actin and actin structures affected by cofilins are flexible in bending and torsion.

twisted structure, and it is known to have a twisting effect when tensile forces are applied.^{1,17} In addition, cofilin is known to increase the torsional flexibility of actin when it is bound to it.⁵⁵ Thus, we expected the cofilactin filament to have a different twisted angle than the actin filament, as well as a different torsional modulus. The torsional modulus results for the two models are described in Fig. 7b. The torsional modulus of the actin filament maintained a value of about 150 MPa for the seven models with different lengths, and this behavior agreed with that of the fibril-shaped structures found in other studies.^{39,40}

However, the cofilactin filament demonstrated a unique behavior where the torsional modulus decreased when the length increased. For the shortest filaments (25 nm), the cofilactin and actin did not show a significant difference in their torsional modulus values. However, the cofilactin showed a torsional modulus drop of about 50 MPa, and it was maintained at ~ 100 MPa. It was obvious that the cofilin binding caused the actin filament to have a smaller torsional modulus than the actin filament alone.

We evaluated the persistence lengths of the actin and cofilactin filament depicted in Fig. 7c. The persistence length is a factor that defines the length of a material in relation to its behavior as an elastic beam or a chain. It is a mechanical property that can show the difference between actin and cofilactin filaments. We measured the persistence length using eqn (8), which considers the correlation factor measured by the tangential angle of the actin filament. Measuring the persistence length using this process made it possible to compare the simulation results with experimental results from the viewpoints of the structural and mechanical properties. As previously mentioned, the actin and cofilactin filaments in our simulation appeared to have different tangential angles because the cofilactin had a bent form after the equilibration process. Therefore, the correlation factor showed different values for the two models, and the persistence length followed this flow. The persistence length of the actin filament approximately doubled, increasing from 5 to 10.5 μm , when the filament length increased. The persistence length of the actin filament stabilized when the length reached 100 nm. The experimental results gave an actin-filament persistence length of $9.8(\pm 0.14)$ μm , which was practically the same as our measurement.⁵⁶ This was due to the correlation factor of the actin filament, where a pure actin filament maintained a value greater than 0.9 with a filament length of up to 3 μm . The simulation result showed that the actin filament had a correlation factor of one, which meant it had a straight filament form. The cofilactin filament had a smaller persistence length of 6.5 μm , which was smaller than that of the actin filament. This indicated that the range in which the cofilactin worked as an elastic beam was shorter than that of the actin filament, and must be related to the cofilin binding effect. However, in the experimental results, the persistence length of the cofilactin was smaller than ours at $2.2(\pm 0.026)$ μm .⁵⁶ This was related to the configuration of the cofilactin with a long length. For an experimental result, the correlation factor for a cofilactin filament up to a length of ~ 5.5 μm was calculated, and it started from 1 and dropped to ~ 0.28 . Compared to the actin filament, this is a huge drop in the correlation factor, which indicated that the configuration of the cofilactin filament was much more bent. Compared to the experimental model, our simulation model's maximum length was just about 180 nm. Even the experimental cofilactin filament had a large correlation factor for this short length, similar to our simulation model. Thus, considering the limitation on the total length of the cofilactin filament and the relationship with the correlation factor, the persistence length measured with our model was reasonable. However, it would be more meaningful to measure the persistence length for a longer filament to show the change due to cofilin binding.

Discussion

In this study, we examined the mechanical properties of actin and cofilactin filaments and analyzed cofilin's effect on an actin filament using a CGMD simulation with MARTINI and an ENM. The CGMD results demonstrated that cofilin causes the actin filaments to be more twisted and crooked from the viewpoint of conformational changes. The ENM results explained that the mechanical properties of actin structures affected by cofilins are smaller than those of pure actin filaments. Those results are similar to the results of various experimental or simulation methods. Therefore, this study is beneficial because it provides fundamental insights and shows that computational calculations are also helpful in explaining biophysical phenomena and experimental conclusions in a very efficient manner. Unfortunately, there are many voices arguing that computer simulations, especially with an ENM, have limitations and cannot exactly verify the biological roles or functions of bio-structures. The reasons are based on the fact that an ENM only manipulates the positions of alpha-carbon atoms located at a subjectively fixed cutoff distance, which is also drastically coarse grained, and the information is based on PDB, which is not equilibrated. In order to overcome these issues and verify the reliability of our work, we carefully compared the mechanical properties of actin filaments with a large quantity of experimental data and also applied MD simulations to stabilize the positions of the atoms saved in the PDB. Even though the size of the actin filaments was too large to use an all-atom MD simulation, MARTINI (CGMD simulation) was applied instead, and we successfully equilibrated the positions of the atoms and used these as a basis for structuring the ENM.

However, there were still limitations due to using the ENM in our research. Our results showed that our cofilactin filament fit the configuration behavior found in experimental results, but it was obvious that we did not make longer filaments that included cofilin. Therefore, we might have missed some chemical effects that occur when cofilin is bound to actin in longer filaments. However, a large quantity of computational resources is required to simulate a large filament structure such as actin. Our approach is another way to consider large structures such as actin filaments.

In conclusion, coarse-grained MD results and ENM results could provide data similar to experimental results and explain the general conformational change tendency when cofilin was added to actin filaments. Furthermore, it would be possible to simulate the mechanical properties of cofilactin, including cofilin, using such CGMD methods, or to enlarge the filament structure using the data obtained from computational studies.

Acknowledgements

This research was supported by Basic Science Research Program through the National Research Foundation of Korea (NRF) funded by the Ministry of Science, ICT & Future Planning (MSIP) (No. 2007-0056094) and (No. 2013-055175).

References

- 1 S. Matsushita, Y. Inoue, M. Hojo, M. Sokabe and T. Adachi, *Journal of Biomechanics*, 2011, **44**, 1776–1781.
- 2 T. D. Pollard and G. G. Borisy, *Cell*, 2003, **112**, 453–465.
- 3 T. D. Pollard and J. Berro, *J. Biol. Chem.*, 2009, **284**, 5433–5437.
- 4 N. Watanabe and T. J. Mitchison, *Science*, 2002, **295**, 1083–1086.
- 5 T. M. Svitkina, A. B. Verkhovskiy, K. M. McQuade and G. G. Borisy, *J. Cell Biol.*, 1997, **139**, 397–415.
- 6 J. Rosenblatt, P. Peluso and T. Mitchison, *Mol. Biol. Cell*, 1995, **6**, 227–236.
- 7 M.-F. Carlier, *Int. Rev. Cytol.*, 1989, **115**, 139–170.
- 8 T. Pollard, *Curr. Opin. Cell Biol.*, 1990, **2**, 33–40.
- 9 A. Michelot, J. Berro, C. Guérin, R. Boujemaa-Paterski, C. J. Staiger, J.-L. Martiel and L. Blanchoin, *Curr. Biol.*, 2007, **17**, 825–833.
- 10 J. Condeelis, *Trends Cell Biol.*, 2001, **11**, 288–293.
- 11 B. R. McCullough, E. E. Grintsevich, C. K. Chen, H. Kang, A. L. Hutchison, A. Henn, W. Cao, C. Suarez, J.-L. Martiel and L. Blanchoin, *Biophys. J.*, 2011, **101**, 151–159.
- 12 D. Pavlov, A. Muhlrads, J. Cooper, M. Wear and E. Reisler, *J. Mol. Biol.*, 2007, **365**, 1350–1358.
- 13 P. A. Janmey, S. Hvidt, G. F. Oster, J. Lamb, T. P. Stossel and J. H. Hartwig, 1990.
- 14 A. Kishino and T. Yanagida, 1988.
- 15 S. Matsushita, T. Adachi, Y. Inoue, M. Hojo and M. Sokabe, *Journal of Biomechanics*, 2010, **43**, 3162–3167.
- 16 R. L. Satcher Jr and C. F. Dewey Jr, *Biophys. J.*, 1996, **71**, 109–118.
- 17 S. Matsushita, Y. Inoue and T. Adachi, *Biochem. Biophys. Res. Commun.*, 2012, **420**, 710–713.
- 18 T. D. Romo and A. Grossfield, *Proteins: Struct., Funct., Bioinf.*, 2011, **79**, 23–34.
- 19 M. Rueda, P. Chacon and M. Orozco, *Structure*, 2007, **15**, 565–575.
- 20 A. Perez, Z. Yang, I. Bahar, K. A. Dill and J. L. MacCallum, *J. Chem. Theory Comput.*, 2012, **8**, 3985–3991.
- 21 S. J. Marrink, H. J. Risselada, S. Yefimov, D. P. Tieleman and A. H. de Vries, *J. Phys. Chem. B*, 2007, **111**, 7812–7824.
- 22 L. Monticelli, S. K. Kandasamy, X. Periole, R. G. Larson, D. P. Tieleman and S.-J. Marrink, *J. Chem. Theory Comput.*, 2008, **4**, 819–834.
- 23 T. Haliloglu, I. Bahar and B. Erman, *Phys. Rev. Lett.*, 1997, **79**, 3090.
- 24 I. Bahar, A. R. Atilgan and B. Erman, *Folding Des.*, 1997, **2**, 173–181.
- 25 E. Eyal, C. Chennubhotla, L.-W. Yang and I. Bahar, *Bioinformatics*, 2007, **23**, i175–i184.
- 26 M. M. Tirion, *Phys. Rev. Lett.*, 1996, **77**, 1905.
- 27 A. Atilgan, S. Durell, R. Jernigan, M. Demirel, O. Keskin and I. Bahar, *Biophys. J.*, 2001, **80**, 505–515.
- 28 Z. Yang, P. Májek and I. Bahar, *PLoS Comput. Biol.*, 2009, **5**, e1000360.
- 29 D. Tobi and I. Bahar, *Proc. Natl. Acad. Sci. U. S. A.*, 2005, **102**, 18908–18913.

- 30 I. Bahar and A. J. Rader, *Curr. Opin. Struct. Biol.*, 2005, **15**, 586–592.
- 31 C. Y. Xu, D. Tobi and I. Bahar, *J. Mol. Biol.*, 2003, **333**, 153–168.
- 32 N. Kantarci-Carsibasi, T. Haliloglu and P. Doruker, *Biophys. J.*, 2008, **95**, 5862–5873.
- 33 O. Kurkcuoglu, R. L. Jernigan and P. Doruker, *Polymer*, 2004, **45**, 649–657.
- 34 P. Doruker, R. L. Jernigan and I. Bahar, *J. Comput. Chem.*, 2002, **23**, 119–127.
- 35 J. I. Kim, S. Na and K. Eom, *J. Comput. Chem.*, 2011, **32**, 161–169.
- 36 J.-I. Kim, S. Na and K. Eom, *J. Chem. Theory Comput.*, 2009, **5**, 1931–1939.
- 37 H. Jang, S. Na and K. Eom, *J. Chem. Phys.*, 2009, **131**, 245106.
- 38 K. Eom, S.-C. Baek, J.-H. Ahn and S. Na, *J. Comput. Chem.*, 2007, **28**, 1400–1410.
- 39 G. Yoon, J. Kwak, J. I. Kim, S. Na and K. Eom, *Adv. Funct. Mater.*, 2011, **21**, 3454–3463.
- 40 Z. Xu, R. Paparcone and M. J. Buehler, *Biophys. J.*, 2010, **98**, 2053–2062.
- 41 G. Yoon, Y. Kab Kim, K. Eom and S. Na, *Appl. Phys. Lett.*, 2013, **102**, 011914.
- 42 V. E. Galkin, A. Orlova, D. S. Kudryashov, A. Solodukhin, E. Reisler, G. F. Schröder and E. H. Egelman, *Proc. Natl. Acad. Sci. U. S. A.*, 2011, **108**, 20568–20572.
- 43 W. Humphrey, A. Dalke and K. Schulten, *J. Mol. Graphics*, 1996, **14**, 33–38.
- 44 G. Kresse and J. Hafner, *Phys. Rev. B: Condens. Matter Mater. Phys.*, 1993, **47**, 558.
- 45 H. J. C. Berendsen, D. van der Spoel and R. van Drunen, *Comput. Phys. Commun.*, 1995, **91**, 43–56.
- 46 D. Van Der Spoel, E. Lindahl, B. Hess, G. Groenhof, A. E. Mark and H. J. C. Berendsen, *J. Comput. Chem.*, 2005, **26**, 1701–1718.
- 47 S. Pronk, S. Páll, R. Schulz, P. Larsson, P. Bjelkmar, R. Apostolov, M. R. Shirts, J. C. Smith, P. M. Kasson, D. van der Spoel, B. Hess and E. Lindahl, *Bioinformatics*, 2013, **29**, 845–854.
- 48 B. Hess, C. Kutzner, D. van der Spoel and E. Lindahl, *J. Chem. Theory Comput.*, 2008, **4**, 435–447.
- 49 S. O. Yesylevsky, L. V. Schäfer, D. Sengupta and S. J. Marrink, *PLoS Comput. Biol.*, 2010, **6**, e1000810.
- 50 I. Bahar, A. R. Atilgan, M. C. Demirel and B. Erman, *Phys. Rev. Lett.*, 1998, **80**, 2733.
- 51 L. Meirovitch, *Fundamentals of vibrations*, McGraw-Hill, 2001.
- 52 S. P. Timoshenko and J. N. Goodier, *Theory of elasticity*, McGraw-Hill, 1970.
- 53 J. M. Gere and B. J. Goodno, *Mechanics of Materials*, CENGAGE Learning, 2009.
- 54 J. Fan, M. G. Saunders, E. J. Haddadian, K. F. Freed, E. M. De La Cruz and G. A. Voth, *J. Mol. Biol.*, 2013, **425**, 1225–1240.
- 55 E. Prochniewicz, N. Janson, D. D. Thomas and E. M. De La Cruz, *J. Mol. Biol.*, 2005, **353**, 990–1000.
- 56 B. R. McCullough, L. Blanchoin, J.-L. Martiel and E. M. De La Cruz, *J. Mol. Biol.*, 2008, **381**, 550–558.
- 57 T. P. J. Knowles and M. J. Buehler, *Nat. Nanotechnol.*, 2011, **6**, 469–479.
- 58 F. Oosawa, *Biophys. Chem.*, 1980, **11**, 443–446.
- 59 A. Ott, M. Magnasco, A. Simon and A. Libchaber, *Phys. Rev. E: Stat. Phys., Plasmas, Fluids, Relat. Interdiscip. Top.*, 1993, **48**, R1642.
- 60 F. Gittes, B. Mickey, J. Nettleton and J. Howard, *J. Cell Biol.*, 1993, **120**, 923–934.
- 61 T. Yanagida, M. Nakase, K. Nishiyama and F. Oosawa, 1984.
- 62 R. Yasuda, H. Miyata and K. Kinoshita Jr, *J. Mol. Biol.*, 1996, **263**, 227–236.
- 63 H. Isambert, P. Venier, A. C. Maggs, A. Fattoum, R. Kassab, D. Pantaloni and M.-F. Carlier, *J. Biol. Chem.*, 1995, **270**, 11437–11444.
- 64 D. Riveline, C. H. Wiggins, R. Goldstein and A. Ott, *Phys. Rev. E: Stat. Phys., Plasmas, Fluids, Relat. Interdiscip. Top.*, 1997, **56**, R1330.
- 65 D. E. Dupuis, W. H. Guilford, J. Wu and D. Warshaw, *J. Muscle Res. Cell Motil.*, 1997, **18**, 17–30.
- 66 Y. Tsuda, H. Yasutake, A. Ishijima and T. Yanagida, *Proc. Natl. Acad. Sci. U. S. A.*, 1996, **93**, 12937–12942.
- 67 H. Yoshimura, T. Nishio, K. Mihashi, K. Kinoshita Jr and A. Ikegami, *J. Mol. Biol.*, 1984, **179**, 453–467.
- 68 E. Prochniewicz, Q. Zhang, E. C. Howard and D. D. Thomas, *J. Mol. Biol.*, 1996, **255**, 446–457.
- 69 A. R. Atilgan, S. R. Durell, R. L. Jernigan, M. C. Demirel, O. Keskin and I. Bahar, *Biophys. J.*, 2001, **80**, 505–515.
- 70 J. J. Bravo-Cordero, M. A. O. Magalhaes, R. J. Eddy, L. Hodgson and J. Condeelis, *Nat. Rev. Mol. Cell Biol.*, 2013, **14**, 405–415.
- 71 C. Suarez, J. Roland, R. Boujemaa-Paterski, H. Kang, B. R. McCullough, A.-C. Reymann, C. Guérin, J.-L. Martiel, E. M. De La Cruz and L. Blanchoin, *Curr. Biol.*, 2011, **21**, 862–868.